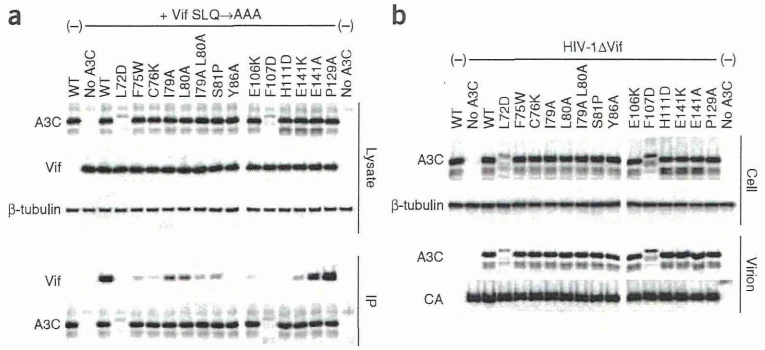

Figure 2 Ten A3C residues critical for HIV-1 Vif interaction. (**a**) Immunoblots of lysates and anti-His immunoprecipitates of HEK-293T cells with wild type (WT), mutant A3C-Myc-His or control plasmid (no A3C) expressed in the presence (+) or absence (–) of HIV-1 Vif SLQ→AAA. Immunoblotting is with anti-Vif or anti-His monoclonal antibodies as shown. Anti–β-tubulin antibody was used as a loading control. IP, immunoprecipitation. (**b**) Virion-packaging efficiency of Vif-resistant A3C mutants. Intracellular (cell) and virus-incorporated (virion) levels of A3C WT and mutants analyzed by western blotting. Samples are from cells transfected with HIV-1ΔVif or control plasmids (–), plus either A3C or control plasmids (no A3C). The HIV-1 capsid protein (CA) levels in virions were detected with an anti-p24 antibody.

E106K substitution changes the susceptibility of A3C to Vif-mediated degradation[10], which suggests that Glu106 is one of the residues responsible for the A3C-Vif interaction. Therefore, to further identify the other critical residues adjacent to Glu106, we first introduced substitution mutations near Glu106 and tested the Vif sensitivity *in vitro*. The results are summarized in **Supplementary Figure 3**. Wild-type A3C was not detectable when coexpressed with Vif (Vif sensitive), whereas the expression of the E106K mutant was unchanged in the presence of Vif (Vif resistant). These experiments were repeated for all residues whose mutations resulted in a Vif-resistant phenotype, until the surrounding A3C surface residues were all associated with sensitive mutants. The percentage reduction of A3C expression in the presence relative to the absence of Vif was evaluated (Vif-resistance level) (**Supplementary Fig. 3**). The results indicated that any single point mutation in the nine residues (Leu72, Phe75, Cys76, Ile79, Leu80, Ser81, Tyr86, Glu106 and Phe107) resulted in a >50% Vif-resistance level, whereas the mutations H111D and A109K resulted in 45% and 41% resistance, respectively. To evaluate whether these residues were intrinsically involved in the Vif interaction, we immunoprecipitated a Vif SOCS-box mutant (Vif SLQ→AAA) that can bind A3 but not EloBC[8,26,27] in the presence of wild-type or Myc-His-tagged A3C mutants, and immunoblotted for Vif SLQ→AAA (**Fig. 2a**). Vif was coimmunoprecipitated with wild-type A3C and A3C P129A at equal levels (**Fig. 2a**), which indicated that Pro129 in A3C is not responsible for the Vif interaction, unlike findings with A3G[16]. In contrast, all of the Vif-resistant A3C mutants immunoprecipitated minimal amounts of Vif, which indicated that the residues whose mutations conferred the Vif-resistant phenotypes are indeed critical for the Vif interaction. The E141K mutation abolished Vif binding, despite being relatively Vif sensitive. The reason for this effect is not clear. These findings demonstrated that Leu72, Phe75, Cys76, Ile79, Leu80, Ser81, Tyr86, Glu106, Phe107 and His111 are involved in forming the Vif-interaction interface. All of the binding-deficient A3C mutants were incorporated into *vif*-deficient HIV-1 (HIV-1ΔVif) as efficiently as wild-type A3C (**Fig. 2b**), which suggested that RNA-binding capacity was not impaired by the A3C mutations.

Structural mapping of the mutagenesis results yielded a Vif-resistance level, which is color-coded on the structure (**Fig. 3a,b**). The residues involved in the Vif interaction are located in an area between the α2 and α3 helices, distal from the Pro129 of the A3G DPD motif[16]. Notably, in the A3C surface representation, the interface is a shallow cavity composed of hydrophobic (Leu72, Ile79 and Leu80) or aromatic (Phe75, Tyr86, Phe107 and His111) residues at the bottom and hydrophilic (Cys76, Ser81 and Glu106) residues at the edges (**Fig. 3a–c**). One notable feature of this cavity is that two potential π interactions can be observed at the bottom, on the basis of the configuration of four aromatic residues (Phe75, Tyr86, Phe107

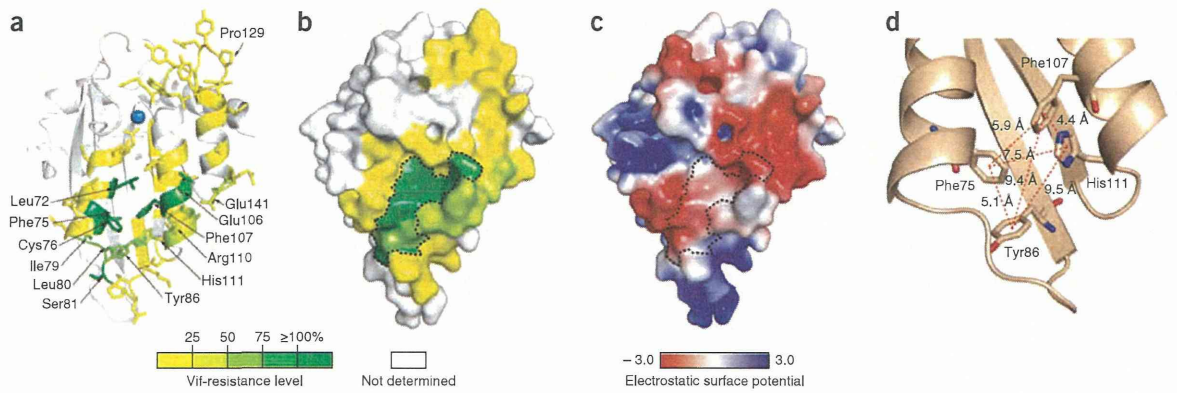

Figure 3 The A3C interface for the HIV-1 Vif interaction. (**a**,**b**) The A3C structure, displaying critical residues for Vif sensitivity. The residues are colored in the ribbon (**a**) and surface (**b**) representations of A3C according to the resistance level of Vif-mediated degradation, as shown in the bottom bar. Residues exhibiting a >50% Vif-resistance level are enclosed by a dotted line. (**c**) The electrostatic potential of A3C is shown. The accessible surface area is colored according to the calculated electrostatic potential from –3 *kT/e* (red) to 3 *kT/e* (blue). The orientation and the dotted line are the same as in **b**. (**d**) Potential π-stacking interactions at the Vif-binding interface in A3C. The distances between the four aromatic residues involved in the Vif-binding cavity (Phe75, Tyr86, Phe107 and His111) are shown.

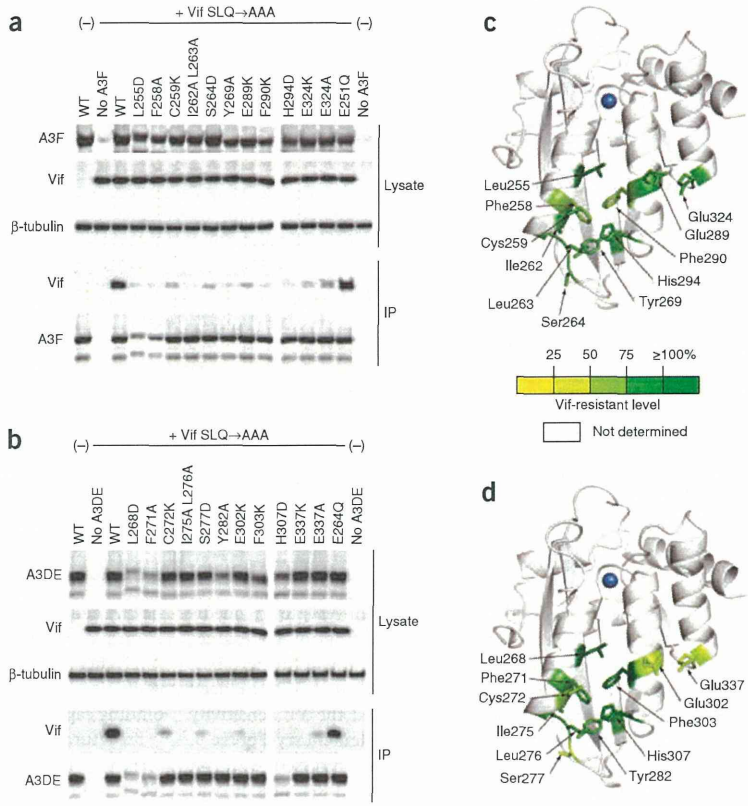

Figure 4 Analogous residues of A3F and A3DE are involved in the HIV-1 Vif-binding interface. (**a**,**b**) Coimmunoprecipitation (IP) of HIV-1 Vif SLQ→AAA with wild type (WT) or A3F-MycHIS mutants (**a**) and with wild type or A3DE-MycHIS mutants (**b**). (**c**,**d**) Residues are mapped on the A3F (**c**) or the A3DE CTD (**d**) structures modeled on the A3C crystal structure. The residues are color coded according to their Vif-resistance levels. A coordinated zinc ion is shown as a blue sphere.

and His111) (**Fig. 3d**). Both Phe75-Tyr86 and Phe107-His111 show the proper distance and orientation to make two weak π-π interactions. In contrast, the pair of Phe75-Phe107 shows theoretically proper distance, although the angle is not appropriate to form a potential interaction. In addition, because a mutation of the hydrophobic or aromatic residues disrupts the Vif interaction and subsequent degradation, a specific size of the hydrophobic side chains, as well as π stacking, may be important for maintaining the correct interface conformation and for the A3C-Vif interaction. The interface includes a flexible region, loop 4, where Cys76, Ile79, Leu80 and Ser81 exhibit higher temperature factors in the crystal-structure data and in the MD simulations (**Supplementary Fig. 1f**), which suggests a partially flexible interface. Furthermore, the electrostatic surface potential analysis revealed a negatively charged interface (**Fig. 3c**), and substitutions with positively charged residues increase the Vif-resistance levels (**Supplementary Fig. 3**), which suggests that the negative electrostatic surface at the interface is also an important feature for HIV-1 Vif binding.

Vif-binding interfaces are conserved in A3C, A3F and A3DE

We also performed analogous coimmunoprecipitation experiments with equivalent mutations in the A3F and A3DE CTDs and tested for Vif interaction (**Fig. 4**). For A3F, involvement of the A3F Glu289 and Glu324 residues in Vif interaction has been reported[10,17]. Coimmunoprecipitates of these A3F mutants contained significantly reduced amounts of Vif (**Fig. 4a**) compared to wild type or E251Q (a mutation at the catalytic center), which demonstrates that the equivalent residues of A3F, Leu255, Phe258, Cys259, Ile262, Leu263, Ser264, Tyr269, Glu289, Phe290 and His294, are also important for the Vif interaction. In addition, we assessed the Vif sensitivity of the mutants (**Supplementary Fig. 3c**,**e**) and mapped the residues onto a homology model of the A3F CTD (**Fig. 4c**). Again, these residues were clustered and formed a Vif-binding cavity homologous to that observed in the A3C structure, although a slight difference in the Vif-resistant phenotype was observed. The E141K A3C mutant displayed a low Vif-resistance level (27%), whereas the corresponding A3F mutant, E324K, had a high resistance level (87%) (**Supplementary Fig. 3c**,**e**). MD simulations suggested that conformational differences at the negatively charged edge of the cavity may be responsible for these differences (**Supplementary Fig. 4**).

For A3DE, the analysis of the coimmunoprecipitation assays demonstrated that 10 equivalent residues (Leu268, Phe271, Cys272, Ile275, Leu276, Ser277, Tyr282, Glu302, Phe303 and His307) of A3DE are also important for Vif interaction (**Fig. 4b**). In addition, mutations at any of the residues critical for Vif interaction resulted in a Vif-resistant phenotype, although the A3DE S277D and E302K mutants presented a lower of the Vif-resistance than the equivalents of A3F S264D and E289K, respectively (**Supplementary Fig. 3c–f**). Moreover, these residues provide a similar Vif-binding interface to that of A3C (**Fig. 4d**). These results suggest that the conformation of the Vif-interaction interface is highly conserved among A3C and the CTDs of A3F and A3DE.

To further assess whether the Z2-type A3G NTD provides a similar Vif-interaction interface at the equivalent position between the α2 and α3 helices, we constructed four analogous A3G mutants, F74W, L80D, Y86A and F107K, that have a substitution at identical residues, on the basis of sequence alignments between A3C and the A3G NTD. Examination of Vif sensitivity in these mutants indicated that none of these mutations in the A3G NTD changed the Vif-sensitive phenotype (**Supplementary Fig. 5**). These results demonstrated that the Vif-binding interface of A3G NTD is distinct from that of A3C, A3F and A3DE. In addition, they suggest that mutations between the α2 and α3 helices do not distort the presumed Vif-binding interface conformation of the A3G NTD.

Vif-resistant A3F inhibits HIV-1 infection

To elucidate the effects of the A3F mutations on viral incorporation, we analyzed the amounts of wild-type and mutant A3F proteins in cells and virions. Both wild-type and mutant A3F were efficiently incorporated into virus particles, with the exception of the H294D

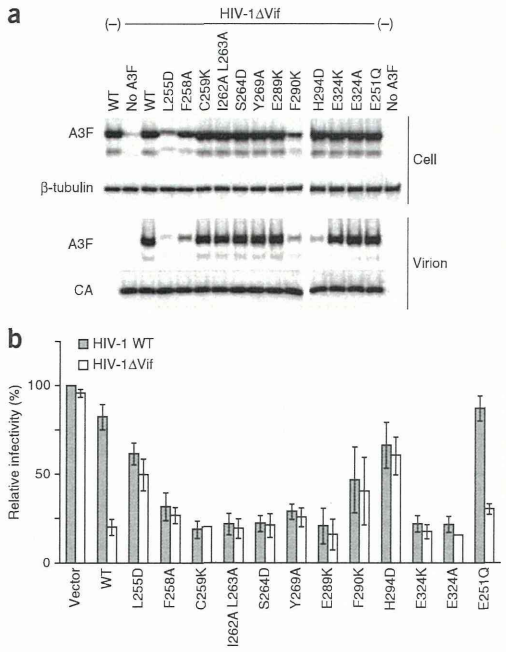

Figure 5 The effects of mutations at the equivalent residues in A3F on antiviral activity. (**a**) Intracellular expression (cell) and incorporation of wild-type A3F and the mutants into virions (virion), evaluated by western blotting. The CA level in virions was detected by an anti-p24 antibody. (**b**) The antiviral effects of A3F and mutants on wild-type HIV-1 (HIV-1 WT) or HIV-1ΔVif in a single-round replication assay with LuSIV cells. The relative viral infectivity of wild-type HIV-1 in the absence of A3F (vector) was set to 100%. Relative infectivity data are shown as means ± s.d. of three independent experiments.

mutant (**Fig. 5a**). This result suggests that the critical residues for Vif interaction (except for His294) of A3F are not located in the region that is responsible for A3F packaging into virions. Finally, to evaluate whether the A3F mutants exhibited any antiviral activity against HIV-1, we compared the infectivity of wild-type HIV-1 and HIV-1ΔVif in the presence of wild-type or mutant A3F. The wild-type A3F and the E251Q mutant reduced HIV-1ΔVif infectivity to 21% and 30%, respectively, whereas wild-type HIV-1 infectivity was only marginally affected (**Fig. 5b**). In contrast, all of the Vif-resistant A3F mutants suppressed the infectivity of wild-type HIV-1 as efficiently as for HIV-1ΔVif, which is consistent with their packaging level (**Fig. 5a,b**). These findings demonstrate that a disruption of the A3F-Vif interaction prevents A3F degradation and thereby allows A3F to be efficiently packaged into HIV-1 virions to exert its antiviral activity.

DISCUSSION

Studies conducted over the past decade have established that HIV-1 Vif abolishes the antiviral activity of A3 by recruiting an E3 ubiquitin ligase complex to promote proteasomal degradation. Many efforts toward developing strategies that interfere with the A3-Vif interaction have been unsuccessful to date, in part because of the lack of available structural information on the A3-Vif interaction interface. Here, we present, to our knowledge, the first crystal structure of A3C containing an HIV-1 Vif-interaction interface. In addition, our extensive structure-guided mutagenesis revealed the precise Vif-interaction site, between the α2 and α3 helices of A3C, and permitted the delineation of structural features (negatively charged, hydrophobic and partially flexible) in the Vif-interaction interface. Additional investigations demonstrated that the Vif-binding interfaces are highly conserved among Z2-type cytidine deaminases, including A3C, A3F and A3DE, but not A3G.

In combination with the A3C structure, our results suggest that the Vif-interaction interface forms a shallow cavity that is composed of hydrophobic and negatively charged residues. Notably, the positively charged DRMR motif (residues 14–17)[26] and hydrophobic residues (Leu24, Val25, Leu64, Ile66 and Leu72) on HIV-1 Vif are required for its specific interaction with A3C (reviewed in ref. 28), thereby confirming that both the electrostatic and hydrophobic interactions are the fundamental driving force for the A3C-Vif interaction. In addition, Vif Trp5, Trp21, Trp38, Tyr69, Trp70 and Trp89 are commonly considered essential for the interaction with A3C, A3F, A3DE or A3G. These data suggest that the π interactions of the aromatic residues between the A3C interface and Vif may contribute to their association, and these interactions are presumably common to all A3-Vif interactions. Recent reports indicate that Vif Trp21 and Trp38 are important for binding with the cofactor CBF-β. The π interactions may be mediated by CBF-β for efficient formation of the E3 ubiquitin ligase complex[4,5,29]. In addition, the existence of a partially flexible region in the Vif-binding interface (**Supplementary Fig. 1f**) suggests that the cavity may not locally exhibit a fixed conformation, and certain structural changes may be induced by Vif to allow a tight interaction.

Although the A3G NTD is categorized as a Z2-type cytidine deaminase, the amino acid sequences of the A3G NTD and A3C are quite different; only 42.8% of the A3C sequences are identical to the A3G NTD, whereas 77% and 76% are identical to the A3F CTD and A3DE CTD sequences, respectively. In particular, the residues of the α2–α3 regions are not homologous between A3C, A3F, A3DE and the A3G NTD, which suggests differences in their local conformations. For A3C, the Vif-binding interface is located in a region distal to loop 7 that corresponds to an area of the DPD motif in the A3G NTD. In addition, our homologous mutagenesis showed that the equivalent area of the A3G NTD between the α2 and α3 helices is not critical for the A3G-Vif interaction (**Supplementary Fig. 5**), demonstrating that two different regions in A3C and the A3G NTD molecules participate in each specific interaction with Vif. The presence of these distinct interfaces is consistent with the evidence that the HIV-1 Vif residues responsible for binding to A3 proteins are different. The YRHHY motif (residues 40–44) and the DRMR motif in Vif are involved in specific interactions with A3G, and A3C, A3F or A3DE, respectively[11,26,30–33]. Nevertheless, because both types of A3-Vif interactions fundamentally require electrostatic and hydrophobic bindings and the involvement of the flexible loop conformations (loop 4 for A3C, A3F or A3DE; loop 7 for A3G), the interfaces of A3C, A3F or A3DE and A3G may have similar structural characteristics.

Our determination of the high-resolution A3C crystal structure and extensive structure-guided mutagenesis revealed the A3C structural features associated with the Vif interaction. In addition, the conformation of the Vif-binding interface is highly conserved within the Z2-type A3 subfamily. The location of the Vif-binding interface on A3 proteins may prove to be important during the development of pharmacologic agents that target A3-Vif interactions. Previous reports have shown that the residues of A3G and A3C that are critical for nucleic acid binding also have essential roles in the efficient packaging

of A3 into virions[16,34]. These residues are involved in the formation of nucleic acid–binding grooves primarily consisting of loops 1, 3, 5 and 7 near the coordinated zinc ions of A3G and A3C proteins. The A3G DPD motif for Vif interaction is immediately adjacent to the four YYFW residues (124–127) necessary for A3G incorporation into virions[16]. Therefore, we must use caution to not perturb the contributions of the neighboring YYFW residues that are necessary for A3G incorporation into virions. In contrast, the Vif-binding interfaces that we identified in A3C, A3F and A3DE are mapped to a position distal to the nucleic acid–binding pocket that is important for A3's encapsidation into virions. Therefore, during drug discovery and development, it could be advantageous to target the interaction of Vif with A3C, A3F or A3DE, particularly that with A3F, without disturbing the nucleic acid–binding capability. Taken together, these findings on the structural features of Vif-binding interfaces may aid in our understanding of Vif-A3 interactions and lead to the development of new pharmacologic anti-HIV-1 compounds that could restore the activity of the intrinsic antiviral factor in the context of HIV-1 infection.

METHODS

Methods and any associated references are available in the online version of the paper.

Accession codes. Coordinates and structure factors have been deposited into the Protein Data Bank, with the accession code 3VOW.

Note: Supplementary information is available in the online version of the paper.

ACKNOWLEDGMENTS

We thank A.M. Gronenborn, J.G. Levin and K. Strebel for critical discussions and reading of the manuscript. We also thank K. Tokunaga (National Institute of Infectious Diseases, Tokyo, Japan) for providing the pCAGGS APOBEC3 plasmids. This work was supported in part by a grant from the Ministry of Education, Culture, Sports, Science and Technology of Japan to Y.I. (JSPS KAKENHI 24590568) and by a grant for HIV/AIDS research from the Ministry of Health, Labor and Welfare of Japan to Y.I.

AUTHOR CONTRIBUTIONS

S.K., H.O., M.N., T.K., T.Y., N.W., A.S. and Y.I. performed experiments and analysis for the crystal structure determination; S.K., M.N., M.I., Y.N., T.K., Y.Y. and Y.I. performed biochemical experiments; S.K., M.N., M.I., Y.N., Y.Y., W.S. and Y.I. analyzed the biochemical data; Y.I. directed the project; S.K., H.O. and Y.I. wrote the manuscript with all authors' help.

COMPETING FINANCIAL INTERESTS

The authors declare no competing financial interests.

Published online at http://www.nature.com/doifinder/10.1038/nsmb.2378.
Reprints and permissions information is available online at http://www.nature.com/reprints/index.html.

1. Goila-Gaur, R. & Strebel, K. HIV-1 Vif, APOBEC, and intrinsic immunity. *Retrovirology* **5**, 51 (2008).
2. LaRue, R.S. *et al.* Guidelines for naming nonprimate APOBEC3 genes and proteins. *J. Virol.* **83**, 494–497 (2009).
3. Wedekind, J.E., Dance, G.S., Sowden, M.P. & Smith, H.C. Messenger RNA editing in mammals: new members of the APOBEC family seeking roles in the family business. *Trends Genet.* **19**, 207–216 (2003).
4. Jäger, S. *et al.* Vif hijacks CBF-β to degrade APOBEC3G and promote HIV-1 infection. *Nature* **481**, 371–375 (2012).
5. Zhang, W., Du, J., Evans, S.L., Yu, Y. & Yu, X.F. T-cell differentiation factor CBF-β regulates HIV-1 Vif-mediated evasion of host restriction. *Nature* **481**, 376–379 (2012).
6. Marin, M., Rose, K.M., Kozak, S.L. & Kabat, D. HIV-1 Vif protein binds the editing enzyme APOBEC3G and induces its degradation. *Nat. Med.* **9**, 1398–1403 (2003).
7. Sheehy, A.M., Gaddis, N.C. & Malim, M.H. The antiretroviral enzyme APOBEC3G is degraded by the proteasome in response to HIV-1 Vif. *Nat. Med.* **9**, 1404–1407 (2003).
8. Yu, X. *et al.* Induction of APOBEC3G ubiquitination and degradation by an HIV-1 Vif-Cul5-SCF complex. *Science* **302**, 1056–1060 (2003).
9. Russell, R.A., Smith, J., Barr, R., Bhattacharyya, D. & Pathak, V.K. Distinct domains within APOBEC3G and APOBEC3F interact with separate regions of human immunodeficiency virus type 1 Vif. *J. Virol.* **83**, 1992–2003 (2009).
10. Smith, J.L. & Pathak, V.K. Identification of specific determinants of human APOBEC3F, APOBEC3C, and APOBEC3DE and African green monkey APOBEC3F that interact with HIV-1 Vif. *J. Virol.* **84**, 12599–12608 (2010).
11. Zhen, A., Wang, T., Zhao, K., Xiong, Y. & Yu, X.F. A single amino acid difference in human APOBEC3H variants determines HIV-1 Vif sensitivity. *J. Virol.* **84**, 1902–1911 (2010).
12. Bogerd, H.P., Doehle, B.P., Wiegand, H.L. & Cullen, B.R. A single amino acid difference in the host APOBEC3G protein controls the primate species specificity of HIV type 1 virion infectivity factor. *Proc. Natl. Acad. Sci. USA* **101**, 3770–3774 (2004).
13. Mangeat, B., Turelli, P., Liao, S. & Trono, D. A single amino acid determinant governs the species-specific sensitivity of APOBEC3G to Vif action. *J. Biol. Chem.* **279**, 14481–14483 (2004).
14. Schröfelbauer, B., Chen, D. & Landau, N.R. A single amino acid of APOBEC3G controls its species-specific interaction with virion infectivity factor (Vif). *Proc. Natl. Acad. Sci. USA* **101**, 3927–3932 (2004).
15. Xu, H. *et al.* A single amino acid substitution in human APOBEC3G antiretroviral enzyme confers resistance to HIV-1 virion infectivity factor-induced depletion. *Proc. Natl. Acad. Sci. USA* **101**, 5652–5657 (2004).
16. Huthoff, H. & Malim, M.H. Identification of amino acid residues in APOBEC3G required for regulation by human immunodeficiency virus type 1 Vif and Virion encapsidation. *J. Virol.* **81**, 3807–3815 (2007).
17. Albin, J.S. *et al.* A single amino acid in human APOBEC3F alters susceptibility to HIV-1 Vif. *J. Biol. Chem.* **285**, 40785–40792 (2010).
18. Chen, K.M. *et al.* Structure of the DNA deaminase domain of the HIV-1 restriction factor APOBEC3G. *Nature* **452**, 116–119 (2008).
19. Furukawa, A. *et al.* Structure, interaction and real-time monitoring of the enzymatic reaction of wild-type APOBEC3G. *EMBO J.* **28**, 440–451 (2009).
20. Holden, L.G. *et al.* Crystal structure of the anti-viral APOBEC3G catalytic domain and functional implications. *Nature* **456**, 121–124 (2008).
21. Shandilya, S.M. *et al.* Crystal structure of the APOBEC3G catalytic domain reveals potential oligomerization interfaces. *Structure* **18**, 28–38 (2010).
22. Betts, L., Xiang, S., Short, S.A., Wolfenden, R. & Carter, C.W.J. Cytidine deaminase. The 2.3 Å crystal structure of an enzyme: transition-state analog complex. *J. Mol. Biol.* **235**, 635–656 (1994).
23. Prochnow, C., Bransteitter, R., Klein, M.G., Goodman, M.F. & Chen, X.S. The APOBEC-2 crystal structure and functional implications for the deaminase AID. *Nature* **445**, 447–451 (2007).
24. Krzysiak, T.C., Jung, J., Thompson, J., Baker, D. & Gronenborn, A.M. APOBEC2 is a monomer in solution: implications for APOBEC3G models. *Biochemistry* **51**, 2008–2017 (2012).
25. Iwatani, Y. *et al.* HIV-1 Vif-mediated ubiquitination/degradation of APOBEC3G involves four critical lysine residues in its C-terminal domain. *Proc. Natl. Acad. Sci. USA* **106**, 19539–19544 (2009).
26. Russell, R.A. & Pathak, V.K. Identification of two distinct human immunodeficiency virus type 1 Vif determinants critical for interactions with human APOBEC3G and APOBEC3F. *J. Virol.* **81**, 8201–8210 (2007).
27. Larue, R.S., Lengyel, J., Jónsson, S.R., Andrésdóttir, V. & Harris, R.S. Lentiviral Vif degrades the APOBEC3Z3/APOBEC3H protein of its mammalian host and is capable of cross-species activity. *J. Virol.* **84**, 8193–8201 (2010).
28. Kitamura, S., Ode, H. & Iwatani, Y. Structural features of antiviral APOBEC3 proteins are linked to their functional activities. *Front. Microbiol.* **2**, 258 (2011).
29. Hultquist, J.F., Binka, M., Larue, R.S., Simon, V. & Harris, R.S. Vif proteins of human and simian immunodeficiency viruses require cellular CBFβ to degrade APOBEC3 restriction factors. *J. Virol.* **86**, 2874–2877 (2012).
30. He, Z., Zhang, W., Chen, G., Xu, R. & Yu, X.F. Characterization of conserved motifs in HIV-1 Vif required for APOBEC3G and APOBEC3F interaction. *J. Mol. Biol.* **381**, 1000–1011 (2008).
31. Pery, E., Rajendran, K.S., Brazier, A.J. & Gabuzda, D. Regulation of APOBEC3 proteins by a novel YXXL motif in human immunodeficiency virus type 1 Vif and simian immunodeficiency virus SIVagm Vif. *J. Virol.* **83**, 2374–2381 (2009).
32. Schröfelbauer, B., Senger, T., Manning, G. & Landau, N.R. Mutational alteration of human immunodeficiency virus type 1 Vif allows for functional interaction with nonhuman primate APOBEC3G. *J. Virol.* **80**, 5984–5991 (2006).
33. Tian, C. *et al.* Differential requirement for conserved tryptophans in human immunodeficiency virus type 1 Vif for the selective suppression of APOBEC3G and APOBEC3F. *J. Virol.* **80**, 3112–3115 (2006).
34. Stauch, B. *et al.* Model structure of APOBEC3C reveals a binding pocket modulating ribonucleic acid interaction required for encapsidation. *Proc. Natl. Acad. Sci. USA* **106**, 12079–12084 (2009).

ONLINE METHODS

Plasmids and antibodies. To construct a plasmid to express A3C in bacteria, a DNA fragment (573 base pairs) was inserted into pET41a(+) (Novagen), which has an N-terminal GST tag and an enterokinase cleavage site. This construct was designated pET41 GST-A3C. A3 expression plasmids for mammalian cells were constructed by replacing the A3G gene of pcDNA A3G (Myc-His)[35] with the cDNA fragments of the A3 derived from pCAGGS APOBEC3 (ref. 36). Substitutions of the A3 residues were introduced into the A3 expression plasmids as previously described[25]. pcDNA-HVif SLQ→AAA was generated by site-directed mutagenesis from pcDNA-HVif[37]. For all mutants, the sequences of both the insert and the boundary regions were verified by DNA sequencing. The pNL4-3 WT and pNL4-3*vif*(−) plasmids were described previously[25]. Anti-p24 (CA) rabbit serum (4250) and a peptide antibody (C-17 rabbit serum; 10082) for human A3G were obtained from the AIDS Research and Reference Reagent Program, National Institute of Allergy and Infectious Diseases, US National Institutes of Health, Germantown, Maryland, USA. Anti-His mAb (D291-3) and anti-His rabbit serum (PM032) (Medical & Biological Laboratories Co.) and anti-Vif mAb (ab66643) and anti–β-tubulin rabbit polyclonal antibody (ab6046; Abcam) were purchased.

Protein expression and purification. Rosetta2(DE3)pLysS bacterial cells (Novagen) transformed with pET41 GST-A3C, were grown at 37 °C in Luria-Bertani medium containing 25 μg ml^{-1} of kanamycin and 34 μg ml^{-1} of chloramphenicol until reaching an optical density at 600 nm (OD_{600}) of 0.6. After the addition of 1 mM IPTG and 1 μM $ZnSO_4$, the cells were further incubated to express the GST-A3C at 20 °C for 20 h. The bacterial pellets were collected by centrifugation and resuspended with a lysis buffer (1,000 mM NaCl, 10 mM $CaCl_2$, 1 mM EDTA, 10% glycerol, 5 mM 2-mercaptoethanol (2-ME) and 25 mM HEPES, pH 7.0). The lysed cells were disrupted by sonication and French press and then subjected to centrifugation and filtration. The supernatant was applied to a glutathione Sepharose 4 FF column (GE Healthcare) for affinity purification. The bound GST-A3C was eluted by an elution buffer (500 mM NaCl, 10 mM $CaCl_2$, 10% glycerol, 5 mM 2-ME, 40 mM reduced L-glutathione and 50 mM Tris HCl, pH 8.0). The eluate was digested by recombinant enterokinase (Novagen) in a cleavage buffer (350 mM NaCl, 12 mM $CaCl_2$, 2% glycerol, 1 mM 2-ME, 1% Triton X-100 and 30 mM Tris HCl, pH 7.4) at 20 °C overnight. The digested A3C was purified by using SPXL cation-exchange chromatography (GE Healthcare) with IEX start buffer (10% glycerol, 5 mM 2-ME and 50 mM Tris HCl, pH 8.0) and IEX elution buffer (IEX start buffer containing 1,000 mM NaCl and 200 mM L-arginine hydrochloride (L-Arg HCl)). A3C was further purified by using Superdex-75 gel filtration chromatography (GE Healthcare).

Protein crystallization. The A3C was dialyzed with crystallization buffer (50 mM NaCl, 300 mM L-Arg HCl, 1 mM Tris(2-carboxyethyl)phosphine hydrochloride (TCEP) and 10 mM HEPES, pH 8.0) and then concentrated to approximately 10 mg ml^{-1} by using Amicon Ultra-0.5 ml (Millipore). The initial crystallization screening was performed at 20 °C by using a JCSG-*plus* Screen solution (Molecular Dimensions) containing 300 mM L-Arg HCl by the hanging-drop vapor-diffusion method. A crystal formed in a condition containing 85 mM bicine (pH 9.0), 17% PEG6000 and 300 mM L-Arg HCl. A better-shaped crystal was grown at 20 °C with 300 μl of reservoir solution (14% PEG6000, 300 mM L-Arg HCl and 85 mM bicine, pH 9.0) by the hanging-drop vapor-diffusion method.

Data collection and processing. The crystal was soaked in a cryoprotectant solution (30% PEG6000, 300 mM L-Arg HCl and 85 mM bicine, pH 9.0) for a few seconds and flash cooled in nitrogen gas. Diffraction data sets were collected at 95 K by using synchrotron radiation (λ = 0.98 Å) on beamline BL-17A at the Photon Factory, KEK (Tsukuba, Japan). The data sets were indexed, integrated and scaled using the HKL2000 program package[38].

Analysis of structure data and construction of structure models. The structure was determined by the molecular replacement method, starting with the A3G 191–384-2K3A crystal structure (PDB 3IR2)[21] by using the program MolRep[39] and was manually built with the program COOT[40]. The structure refinement was performed by using REFMAC5 (ref. 41). The refinement statistics data are summarized in **Table 1**. Structure models of the A3F and DE CTDs were constructed on the basis of our A3C crystal structure by using Discovery Studio 3.0 (Accelrys).

Assays for Vif-dependent degradation of A3. A3C, A3F, A3DE or the mutant A3 expression plasmids (2 μg) and pcDNA-HVif or pcDNA 3.1 (−) control (that is, empty) vector (4 μg) were cotransfected into human embryonic kidney cells (293T) in 6-well plates by using FuGENE HD (Roche). At 48 h after transfection, cell lysates were prepared with Laemmli buffer (Bio-Rad) containing 2.5% 2-ME. Cell lysates were subjected to SDS-PAGE, and the proteins were transferred to Immobilon-P membranes (Millipore). The membranes were first incubated with appropriate antibodies as specified and were then incubated with horseradish peroxidase–conjugated secondary antibodies (Pierce). Protein bands were visualized by enhanced chemiluminescence by using SuperSignal West Dura (Pierce) and analyzed using ImageQuant TL (GE Healthcare).

Coimmunoprecipitation assays. To assess the Vif-A3 interaction *in vivo*, a coimmunoprecipitation assay was performed. Briefly, 293T cells were cotransfected with an A3 plasmid containing a lysine-free Myc-His tag and with pcDNA-HVif SLQ→AAA. At 48 h after transfection, the cells were harvested and then lysed in lysis buffer (150 mM NaCl, 1 mM EDTA, 1% Triton X-100, 10 μg ml^{-1} of RNase A in PBS) plus a protease-inhibitor cocktail (Sigma). Protein complexes were immunoprecipitated with anti-His rabbit serum and Protein G-Dynabeads (Invitrogen) at 4 °C. The beads were washed with lysis buffer and then analyzed with anti-His mAb and anti-Vif mAb for A3 protein and Vif, respectively.

Infectivity assays with LuSIV cells. Virus production and analysis of virus infectivity were performed as reported previously[25]. Briefly, to obtain virus particles, HeLa cells were cotransfected with 4 μg of pNL4-3 WT or pNL4-3*vif*(−) plus 2 μg of pcDNA-A3 or pcDNA 3.1 (−) (vector control). Virus infectivity was determined by single-cycle replication assays with LuSIV cells[42], obtained from the AIDS Research and Reference Reagent Program, National Institute of Allergy and Infectious Diseases, US National Institutes of Health, Germantown, Maryland, USA (originally from J.W. Roos and J.E. Clements). Infectivity was calculated by normalizing for the amount of input CA, determined by p24 antigen ELISA (ZeptoMetrix).

Incorporation of A3 proteins into virions. A3 incorporation was analyzed as previously described[25].

35. Kao, S. *et al.* The human immunodeficiency virus type 1 Vif protein reduces intracellular expression and inhibits packaging of APOBEC3G (CEM15), a cellular inhibitor of virus infectivity. *J. Virol.* **77**, 11398–11407 (2003).
36. Kinomoto, M. *et al.* All APOBEC3 family proteins differentially inhibit LINE-1 retrotransposition. *Nucleic Acids Res.* **35**, 2955–2964 (2007).
37. Nguyen, K.L. *et al.* Codon optimization of the HIV-1 *vpu* and *vif* genes stabilizes their mRNA and allows for highly efficient Rev-independent expression. *Virology* **319**, 163–175 (2004).
38. Otwinowski, Z. & Minor, W. Processing of X-Ray diffraction data collected in oscillation mode. *Methods Enzymol.* **276**, 307–326 (1997).
39. Vargin, A. & Teplyakov, A. MOLREP: an automated program for molecular replacement. *J. Appl. Crystallogr.* **30**, 1022–1025 (1997).
40. Emsley, P., Lohkamp, B., Scott, W.G. & Cowtan, K. Features and development of Coot. *Acta Crystallogr. D Biol. Crystallogr.* **66**, 486–501 (2010).
41. Murshudov, G.N., Vagin, A.A. & Dodson, E.J. Refinement of macromolecular structures by the maximum-likelihood method. *Acta Crystallogr. D Biol. Crystallogr.* **53**, 240–255 (1997).
42. Roos, J.W., Maughan, M.F., Liao, Z., Hildreth, J.E. & Clements, J.E. LuSIV cells: a reporter cell line for the detection and quantitation of a single cycle of HIV and SIV replication. *Virology* **273**, 307–315 (2000).

Sites of Action of HIV-1 Vpu in BST-2/Tetherin Downregulation

Juan F. Arias, Yukie Iwabu, and Kenzo Tokunaga*

Department of Pathology, National Institute of Infectious Diseases, Tokyo, Japan

Abstract: The interferon-inducible host restriction factor bone marrow stromal antigen 2 (BST-2/tetherin) blocks the release of human immunodeficiency virus type 1 (HIV-1) by directly cross-linking virions to the membrane of infected cells. This antiviral effect is counteracted by the HIV-1 accessory protein viral protein U (Vpu) through mechanisms that remain unclear. Accumulating evidence suggests that Vpu antagonizes BST-2 by removing it from the plasma membrane; however, neither the cellular sites of interaction nor the effector mechanisms that result in the downregulation of BST-2 cell-surface expression have been fully determined. Based on current evidence regarding the subcellular localization of Vpu and BST-2 and the latter's trafficking defects induced by their interaction, three models have been proposed. In the first, Vpu is hypothesized to block the traffic of newly synthesized BST-2 towards the cell surface by retaining it in the biosynthetic/secretory compartment. The second model suggests that Vpu sequesters BST-2 within intracellular compartments corresponding to recycling endosomes and the *trans*-Golgi network by blocking its recycling after endocytosis. In the third model, we and others have proposed that Vpu directly internalizes BST-2 from the plasma membrane and induces its enhanced endolysosomal trafficking and degradation. As for its intracellular fate, the viral antagonism of BST-2 is likely dependent on the intracellular sequestration, or the proteasomal/lysosomal degradation of the restriction factor. This review summarizes the current advances in our understanding of the cellular pathways and sites of action of Vpu in the downregulation of cell-surface BST-2.

Keywords: HIV-1, Vpu, BST-2, plasma membrane, downregulation, trafficking, *trans*-Golgi network, recycling endosome.

INTRODUCTION

Interferon (IFN)-α-inducible host restriction factors have evolved in mammals as effectors of intrinsic immune responses, providing resistance to infections by directly interfering with the viral life cycle. Four of these host factors restrict the efficiency of HIV-1 replication: the apolipoprotein B mRNA-editing enzyme catalytic polypeptide-like 3 (APOBEC3) family of cytidine deaminases [1]; the α-isoform of the tripartite motif-containing protein 5 (TRIM5α) [2]; bone marrow stromal antigen 2 (BST-2), also known as tetherin or CD317 [3, 4]; and, the most recently described restriction factor, SAM domain HD domain-containing protein 1 (SAMHD1) [5, 6]. To effectively establish a productive infection, HIV-1 has acquired a series of *trans*-acting viral accessory proteins, including Vif and Vpu, to overcome the antiviral activity of these restriction factors. Vif blocks APOBEC3-mediated cytosine deamination in single-stranded DNA, which halts HIV replication. Vpu antagonizes the antiviral effect of BST-2 that bridges the budding virions to the cell membrane, thereby blocking the release of progeny viruses. HIV-1 is able to replicate in human cells because the viral capsid is not effectively recognized by human TRIM5α [2]. In HIV-2 and related simian immunodeficiency viruses (SIVs), the Vpx protein antagonizes SAMHD1, which blocks HIV-1 replication in myeloid cells.

BST-2, the focus of this review, is an IFN-inducible type II membrane glycoprotein that exhibits unusual topology, consisting of a short N-terminal cytoplasmic tail (CT) followed by an α-helical transmembrane (TM) domain, an extended coiled-coil extracellular domain (EC), and a C-terminal glycophosphatidylinositol (GPI) component that serves as a second membrane anchor [7, 8], although the presence of the GPI-anchor has been recently challenged [9]. Interestingly, in mammalian cells, this unusual double-anchor topology has thus far been found only in an isoform of the prion protein [10]. BST-2 was initially identified as a surface marker in terminally differentiated B-cells in patients with multiple myeloma [11, 12] and as a target of Kaposi's sarcoma-associated herpesvirus K5 ubiquitin ligase [13]. Subsequently, this host protein was rediscovered as a restriction factor [3, 4]. BST-2 efficiently blocks the release of a wide range of enveloped viruses by directly tethering viral particles to the membranes of infected cells. The list of viruses restricted by BST-2 continues to grow, including retroviruses [14-16], filoviruses, arenaviruses, paramyxoviruses [17-20], gamma-herpesviruses [21, 22], and rhabdoviruses [23].

The accessory viral protein U (Vpu), encoded in the genome of HIV-1 and a few SIV strains, is a type I transmembrane protein consisting of a short N-terminal domain, a single TM α-helix domain that is also an uncleaved signal peptide, two cytosolic α-helices separated by a short flexible connector loop, and a C-terminal tail. Vpu mediates the degradation of CD4 receptors [24, 25] and enhances the release of progeny virions from virus-producer cells [26-30] by antagonizing the restriction to viral egress imposed by BST-2 [3, 4, 31]. Furthermore, counteraction of BST-2 by Vpu is important for HIV-1 pathogenesis *in vivo* [32-34], indicating that BST-2 is a functionally active restriction factor whose antagonism is required for the establishment of a successful infection *in vivo*. Here, we summarize the current knowledge of the cellular pathways

*Address correspondence to this author at the Department of Pathology, National Institute of Infectious Diseases, Shinjuku-ku, Tokyo 162-8640, Japan; Tel: +81 3 5285 1111; Fax: +81 3 5285 1189;
E-mail: tokunaga@nih.go.jp

1873-4251/12 $58.00+.00

and sites of action of Vpu in downregulation of cell-surface BST-2.

BST-2 LOCALIZATION AND TRANSPORT

In addition to the cell surface, its site of action, BST-2 is found in various cellular compartments, particularly the *trans*-Golgi network (TGN) and recycling endosomes [35-38]. Since current models of the Vpu–BST-2 interaction draw heavily on the cellular localization and trafficking pathways of both proteins, we first describe the physiologic pathways of intracellular BST-2 trafficking. As shown in Fig. (**1**, i and ii), membrane-bound BST-2 is synthesized in the endoplasmic reticulum (ER) and traverses the Golgi cisternae and TGN. The latter acts as an exocytic hub, where outgoing material is sorted and packed into distinct secretory vesicles. Once it reaches the plasma membrane (PM), BST-2 localizes specifically to cholesterol-enriched lipid rafts, binding through its GPI anchor [7, 39-41]. This localization allows BST-2 to effectively tether virus particles, since several enveloped viruses preferentially bud from these microdomains [42-44].

From the PM, BST-2 and other surface markers undergo constitutive endocytosis, followed by their transport to early/sorting and recycling endosomes [45-48], where incoming material is sorted and then sent to different cellular destinations (Fig. **1**, IV). Thus, from this sorting hub, internalized proteins can be recycled directly back to the PM [49-51]. Alternatively, they may be sent to late endosomes and multi-vesicular bodies, where they are subjected to lysosomal degradation (Fig. **1**, V) [52-54], or transported to the biosynthetic/secretory compartments in a process known as retrograde transport [55-57].

These trafficking pathways are regulated by a complex molecular machinery (see Bonifacino *et al.* [58]) that includes small membrane-bound proteins called soluble N-ethylmaleimide-sensitive fusion factor attachment receptors (SNAREs) [59, 60], clathrin adaptor protein (AP) complex members, and small GTPases of the Rab family [61-65]. Evidence suggests that a clathrin-dependent mechanism is required for BST-2 internalization [39, 41] in a process facilitated by the non-canonical dual tyrosine motif at residues 6 and 8 of the BST-2 CT domain. This YxY_{6-8} motif, conserved through all mammalian BST-2 orthologs, is important in determining the protein's trafficking pathways, as it has been shown to interact with both AP-2 and AP-1 complexes, which play a role in directing cargo membrane proteins to clathrin-coated vesicles [65-67]. AP-2 mediates BST-2 internalization at the PM by endocytosis, whereas AP-1 is associated with the transport of BST-2 from recycling endosomes to the TGN [39, 41].

OVERVIEW OF VPU FUNCTION

Vpu has been known to mediate the ubiquitin-induced degradation of CD4 [24], through a conserved phospho-serine motif (DS52GxxS56) in the cytoplasmic domain (CT) of Vpu which recruits β-transducin repeat-containing protein (β-TrCP) and the E3 ligase complex. This results in proteasomal degradation of newly synthesized CD4 receptors [68, 69] in a process coupled to an ER-associated protein degradation (ERAD)-like pathway [70-72]. CD4 receptor degradation minimizes the superinfection of target cells and prevents the retention of Env precursors in the ER, in addition to guaranteeing the release of progeny virions from the PM [73-75]. Vpu was also found to be required for the efficient release of HIV-1 virions from susceptible cell lines. This activity was later shown to be derived from its antagonism of the restriction factor BST-2 [29, 76, 77], which is discussed extensively in the remainder of this review. Two recent reports have described the novel activity of Vpu that interferes with innate cellular immune responses of natural killer and natural killer T cells [78, 79].

Vpu has been shown to localize primarily in endosomes and the TGN [80, 81], where it is thought to interact with BST-2. Expression of Vpu results in reduced levels of BST-2 at the host cell membrane [3, 4, 40, 82, 83] and either degradation [84-88] or sequestration of the host factor in intracellular compartments [36, 89, 90] leading to increased virus release. In previous work, we and others showed that interaction of Vpu with BST-2 depends on their mutual TM domains, leading to downregulation of the latter from the cell surface and subsequent degradation. Evidence for these sequential events comes from data showing that the antiviral activity of BST-2 is restored in the presence of Vpu harboring mutations that disrupt the mutual association of the two proteins through their TM domains [85, 91-94]. However, in certain cell lines (CEMx174, H9) the interaction of Vpu and BST-2 does not effectively reduce the surface levels of the latter in spite of enhanced virion production [90]. This in turn suggests that downregulation at the PM is not the only anti-BST-2 function of Vpu. The implications of this observation remain to be determined in further studies.

SITES AND MODELS OF VPU'S ACTION IN BST-2 DOWNREGULATION

It is widely recognized that Vpu antagonizes BST-2 function as a virion tether by directly mediating the removal of the restriction factor from its site of action at the cell membrane [4, 35, 85, 95, 96]. Although the exact mechanisms of this antagonism are not well understood, current data suggest that APs are required for downregulation of BST-2 from the cell surface [35, 36]. Likewise, we and others have shown that one of the cellular co-factors required for BST-2 downregulation is β-TrCP [36, 84, 85, 88, 97] that regulates either proteasomal, or ubiquitin-dependent lysosomal degradation [98]. However, the requirement appears to be partial because mutations in the β-TrCP-binding motif of Vpu do not entirely abrogate its antagonism of BST-2 [4, 85, 99]. Overall, based on three putative cellular locations (the biosynthetic/secretory pathway, the PM, and the TGN/recycling endosomes) and three probable effector mechanisms (intracellular sequestration and either proteasomal or lysosomal degradation, as described later), several distinct models of the Vpu–BST-2 interaction leading to cell-surface downregulation of BST-2 have been postulated. These are discussed below.

Interference with the membrane transport of newly synthesized BST-2. Current evidence suggests that Vpu antagonizes BST-2 by altering its anterograde transport *via* sequestration in the biosynthetic/secretory pathway, which in

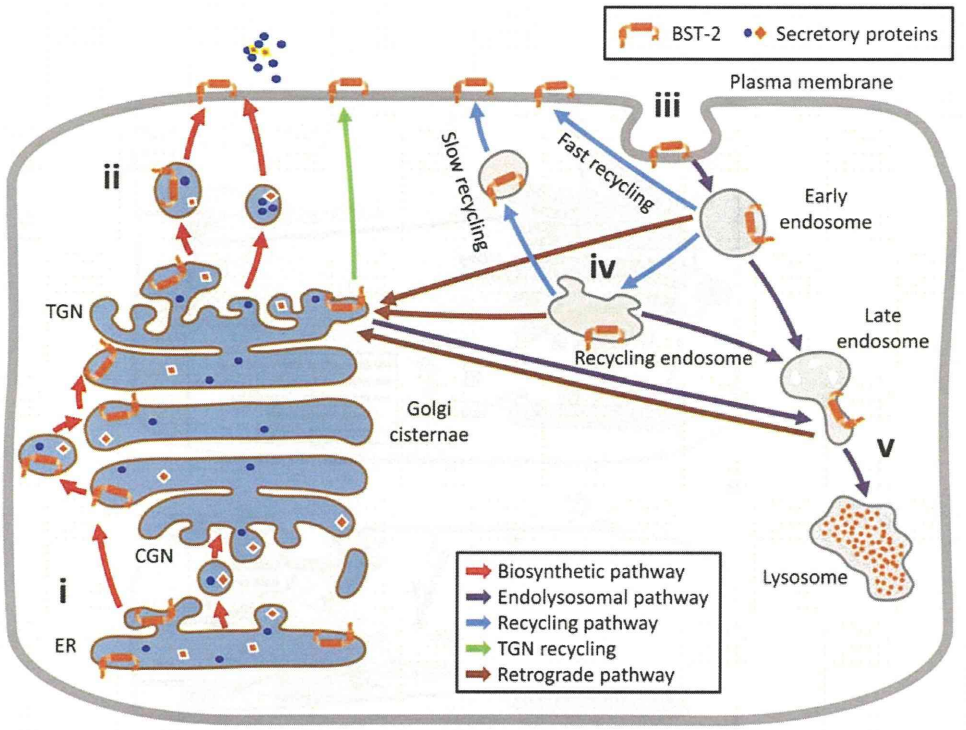

Fig. (1). Physiologic intracellular trafficking pathways of BST-2. Schematic representation of a cell, with the physiologic protein trafficking pathways depicted. The nucleus and other organelles are not shown. The biosynthetic/secretory pathway on the left is represented by red arrows. BST-2 is synthesized in the endoplasmic reticulum (ER) and travels through the *cis*-Golgi network (CGN), Golgi cisternae, and the *trans*-Golgi network (TGN) to finally reach the plasma membrane (PM) *via* secretory vesicles. From the cell surface, BST-2 is internalized, as seen on the right, and then travels either through the endolysosomal pathway, leading to its degradation (purple arrows) or the recycling pathway (blue arrows). The endosomal compartments act as a sorting hub from where BST-2 either cycles directly back to the PM (fast and slow recycling, represented by blue arrows) or relocates to the TGN after which it is sent back to the PM (green arrow). Alternatively, BST-2 can travel through the retrograde pathway (brown arrows), resulting in its transport to the TGN, Golgi membranes, or in some cases even to the ER. Another possibility is that, from recycling endosomes, BST-2 is re-routed to the late endocytic pathway, leading to its degradation in lysosomes.

turn reduces the supply of newly synthesized BST-2 to the cell membrane (Fig. **2A**). The model based on these observations draws support from studies showing that Vpu co-localizes with BST-2 in post-ER membranes [37, 84, 100, 101]. One of these reports has shown that Vpu harboring mutations that altered its intracellular localization and prevented its co-localization with BST-2 in the TGN, is unable to exert its antagonistic effects, suggesting that Vpu targets BST-2 in this compartment [37]. More importantly, Vpu-mediated downregulation of cell-surface BST-2 was strongly attenuated by treatment with Brefeldin A, which blocks ER-to-Golgi transport [37], or with B18R, a vaccinia-encoded antagonist of the type I IFN receptor (since BST-2 synthesis is type I IFN-inducible) [102]. These results suggest that Vpu-induced BST-2 downregulation is dependent on the *de novo* synthesis of the latter protein. It is therefore likely that Vpu blocks the pool of newly synthesized BST-2 which is trafficking to the PM (Fig. **2A**, i), as suggested by subcellular localization studies. BST-2 downregulation might therefore be accomplished simply by its sequestration in the TGN, or alternatively by sorting to the endolysosomal pathway, resulting in its degradation (Fig. **2A**, ii) [86, 102, 103]. Additionally, proteasomal degradation in an ERAD-like process has been suggested as a putative Vpu-mediated degradation mechanism [88] (Fig. **2A**, iii), but the intracellular pathways involved remain to be identified.

Inhibition of BST-2 recycling. Other lines of evidence suggest that Vpu downregulates BST-2 from the plasma membrane, followed by re-localization of the host factor to endosomal (Fig. **2B**, i) and TGN compartments (Fig. **2B**, ii), where BST-2 is sequestered such that its recycling to the cell surface is blocked. Constitutive clathrin-dependent endocytosis mediated by the AP-2 adapter complex [41] or α-adaptin [39] delivers BST-2 to endosomes, where Vpu is located. This results in the sequestration of BST-2 in a post-endocytic compartment and inhibition of its recycling

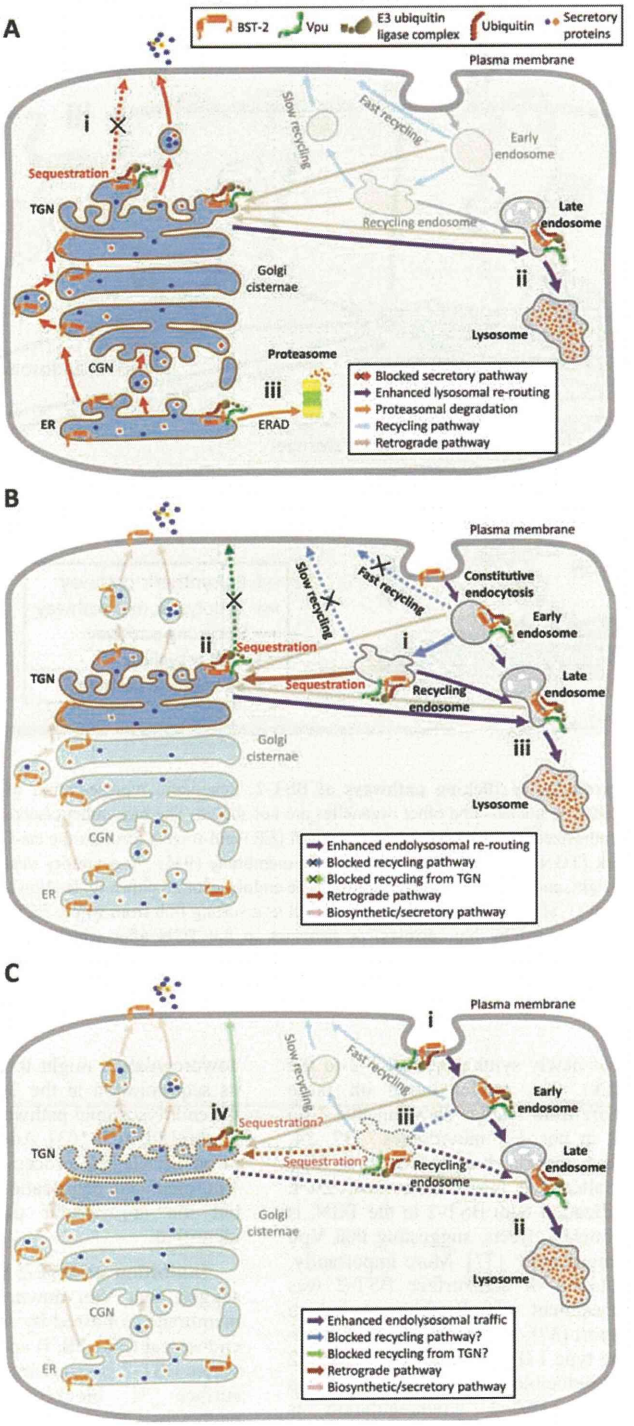
A
BST-2
Vpu
E3 ubiquitin ligase complex
Ubiquitin
Secretory proteins
Plasma membrane
Slow recycling
Fast recycling
Early endosome
Sequestration
TGN
Recycling endosome
Late endosome
Golgi cisternae
Lysosome
Proteasome
CGN
ER
ERAD
Blocked secretory pathway
Enhanced lysosomal re-routing
Proteasomal degradation
Recycling pathway
Retrograde pathway
B
Plasma membrane
Constitutive endocytosis
Early endosome
Sequestration
Recycling endosome
Late endosome
Golgi cisternae
Lysosome
CGN
ER
Enhanced endolysosomal re-routing
Blocked recycling pathway
Blocked recycling from TGN
Retrograde pathway
Biosynthetic/secretory pathway
C
Plasma membrane
Early endosome
Sequestration?
Recycling endosome
Late endosome
Golgi cisternae
Lysosome
CGN
ER
Enhanced endolysosomal traffic
Blocked recycling pathway?
Blocked recycling from TGN?
Retrograde pathway
Biosynthetic/secretory pathway

Fig. (2). Putative sites of interaction and potential alterations of trafficking involved in the downregulation of cell-surface BST-2 by HIV-1 Vpu. Schematic representation of BST-2 trafficking in the presence of Vpu, with the relevant trafficking pathways depicted. The nucleus and other organelles are not shown. (**A**) Vpu-mediated sequestration of BST-2 in biosynthetic/secretory compartments and either subsequent re-routing to the endolysosomal pathway or ERAD-like proteasomal degradation. (**B**) Vpu-mediated blockade of BST-2 recycling, resulting from the sequestration of BST-2 in the TGN and/or recycling endosomes, with subsequent relocation to the endolysosomal pathway for degradation. (**C**) Vpu-mediated direct internalization of BST-2 from the cell surface followed by the consequent enhancement of endolysosomal trafficking or the temporary sequestration of BST-2 in intracellular compartments with its subsequent relocation to the endolysosomal pathway for degradation.

pathway (Fig. **2B**, i) [35, 36, 104]. As discussed above, co-localization studies show that Vpu sequesters BST-2 in the TGN [37, 102, 105]. This trafficking blockade was shown to involve not only the pool of newly synthesized BST-2 but also endocytosed BST-2 recycling back to the cell surface *via* the TGN (Fig. **2B**, ii) [37, 105]. A Vpu-induced defect in BST-2 recycling is supported by the results of flow cytometric assays measuring newly deposited BST-2 at the cell surface. In one study, inhibition of the recycling pathway by the antimalarial drug primaquine induced BST-2 downregulation recapitulating the effect of HIV-1 Vpu expression [105], and in another study, Vpu also inhibited the membrane transport of BST-2 from a brefeldin A-insensitive compartment that presumably corresponds to recycling endosomes [35]. Taken together, these data suggest that inhibition of the BST-2 recycling pathway contributes significantly to Vpu-mediated downregulation of the restriction factor. Indeed, Vpu causes the relocation of BST-2 to an intracellular compartment containing transferrin, a marker of recycling endosomes (Fig. **2B**, i) [35]. This finding is complemented by recent studies showing the subcellular localization of Vpu and BST-2 in the TGN and recycling endosomes [36, 81, 102]. Taken together, these studies support a model in which Vpu interacts with BST-2 in intracellular compartments, most likely recycling endosomes (Fig. **2B**, i) and the TGN (Fig. **2B**, ii), effectively preventing the recycling transport of BST-2. From these compartments, BST-2 is subsequently re-routed to the endolysosomal pathway, ultimately resulting in its lysosomal degradation (Fig. **2B**, iii) [86, 102, 103].

Direct internalization of BST-2 from the cell surface. Although it is clear that Vpu-mediated antagonism requires the downregulation of BST-2 cell-surface expression, the precise role of the cellular internalization machinery in this process is unclear. We previously found that Vpu internalizes BST-2 from the plasma membrane. Overexpression of a dominant-negative form of dynamin-2, which inhibits both clathrin-dependent and -independent endocytosis, abrogated the Vpu-mediated downregulation of cell-surface BST-2 [85]. Our data is supported by reports showing that the Vpu-mediated BST-2 downregulation was inhibited by either siRNA suppression of AP-2 [36], or by the C-terminal fragment of the clathrin assembly protein AP180 [35]. Additionally, we have shown that a constitutive endocytosis-deficient BST-2 mutant harboring mutations in the non-canonical YxY motif of the CT domain [41] is still sensitive to Vpu-induced downregulation [85]. However, it has been recently reported that the rate of constitutive endocytosis in this mutant is not completely impaired [35].

Furthermore, although some reports suggest that Vpu does not upregulate the rate of BST-2 internalization [36, 37, 90], those studies were performed at steady-state and therefore potentially overlooked the early effects of Vpu on the downregulation of cell-surface BST-2. To overcome this limitation, we detected the continuous *de novo* cell-surface expression of BST-2 to enable its visualization at very low levels. The 37°C preincubation during the antibody internalization assay allowed us to detect the direct internalization of cell-surface BST-2 in the presence of Vpu [96]. Dube *et al.* validated this approach in a recent report employing similar conditions [102]. They showed that Vpu enhances the cell-surface clearance of BST-2, moderately in HeLa cells but, more importantly, significantly in $CD4^+$ Jurkat T-cells, the natural HIV-1 target. This suggests that Vpu-induced internalization is cell-type specific, which might depend upon unknown cellular cofactor(s). Taken together, these data suggest that Vpu directly and actively internalizes BST-2 from the PM (Fig. **2C**, i). We also observed that, upon Vpu-mediated internalization, BST-2 trafficking towards the endolysosomal compartment is enhanced, resulting in degradation of the host factor (Fig. **2C**, ii) [85]. It is nonetheless possible that other intracellular sorting pathways (i.e., retrograde and recycling transport) become involved after BST-2 internalization from the PM, resulting in temporary sequestration of the restriction factor in recycling endosomes (Fig. **2C**, iii) or the TGN (Fig. **2C**, iv), with subsequent re-routing to the endolysosomal pathway (Fig. **2C**, ii) for final degradation [86, 102, 103].

INTRACELLULAR FATE OF BST-2 IN THE PRESENCE OF VPU

In addition to the three potential sites of Vpu-BST-2 interaction, three different effector mechanisms have been proposed to account for the Vpu-induced downregulation of cell-surface BST-2, as follows; 1) intracellular sequestration; 2) proteasomal degradation; 3) lysosomal degradation. First, the inhibitory effects of Vpu on BST-2 do not necessarily involve degradation. It has been shown that Vpu decreases total cellular BST-2 levels to a lesser extent than cell-surface BST-2 [36, 89, 90]. As described above, co-localization studies suggest that the downregulation of surface BST-2 depends on Vpu-induced re-localization and accumulation in intracellular compartments overlapping with markers of the TGN [38, 103] or recycling endosomes [35, 36, 104]. Such accumulation could involve the pool of internalized BST-2 recycling back to the cell surface, or the newly synthesized protein in the biosynthetic pathway. Thus, Vpu might sequester BST-2 intracellularly, effectively preventing its constitutive trafficking towards its site of action at the PM.

On the other hand, increasing evidence supports the importance of a degradation pathway in BST-2 antagonism by a mechanism that is dependent upon β-TrCP [36, 84, 85, 88, 97]. It has been shown that the use of proteasomal